cytochalasin D or 0–5 mM amiloride (all from Sigma-Aldrich, St Louis, MO, USA). After the PTD-FAMs were added, cells were maintained for 1 h (30 min for amiloride) in the presence of inhibitors and washed several times with phosphate-buffered saline. As a control, the cellular uptake of transferrin fluorescein isothiocyanate (Invitrogen) was also monitored.

Cell proliferation assay

Cell viability was determined using a WST-8 assay kit (Nacalai Tesque, Kyoto, Japan) according to the manufacturer's instructions. The assay is based on the cleavage of the tetrazolium salt WST-8 to formazan by cellular mitochondrial dehydrogenase. HeLa cells were cultured in 96-well plates (Nalge Nunc International) at 5.0×10^3 cells per well in MEMα and incubated for 24 h at 37 °C. Jurkat cells were cultured in 96-well plates at 1.0×10^4 cells per well in Dulbecco's modified Eagle's medium. The cells were treated with various concentrations of PTD-biotin. After 24 h incubation, cell viability was measured using the WST-8 assay kit.

Membrane integrity assay

The lactate dehydrogenase (LDH) leakage assay was used to quantify the membrane integrity of the PTD-treated cells. This assay detects the amount of LDH released into the culture media as a result of plasma membrane disruption after PTD treatment. HeLa cells were cultured in 96-well plates (Nalge Nunc International) at 5.0×10^3 cells per well in MEMα and incubated for 24 h at 37 °C. Jurkat cells were cultured in 96-well plates at 1.0×10^4 cells per well in Dulbecco's modified Eagle's medium. Each cell type was treated with various concentrations of PTD-biotin. After 3 h incubation, the LDH release activity of the peptides was measured using an LDH cytotoxicity test (Wako) according to the manufacturer's instructions.

Expression and purification of PTD-fused Venus protein

The Venus (variant of yellow fluorescent protein) DNA sequence was kindly provided by Dr A Miyawaki (RIKEN Brain Science Institute). The Tat-Venus DNA sequence was amplified by PCR. At the 5′ end, the primer sequence 5′-TTTAAGAAGGAGATATACATATGGCTTACGGTCGTAAAAAA CGTCGCCAGCGTCGCCGTGGTGGCGGCGGTTCCCTCGA GCACCACCATCACCACCATGTGAGCAAGGGCGAGGAGC TGTTCAC-3′ introduced an *Nde* I site and Tat sequence and at the 3′ end, the primer sequence 5′-GCTTTGTTAGCAG CCGAATTCTTACTTGTACAGCTCGTCCATGCCGAGAGTGA TC-3′ introduced an *Eco* RI site. The PCR product was digested with *Nde* I and *Eco* RI and inserted into a protein expression plasmid. Other plasmids expressing Antp-, Rev- or VP22-Venus recombinant proteins were constructed by replacing the Tat-coding region in the Tat-Venus plasmid with the Antp, Rev or VP22 sequences using the *Nde* I and *Xho* I restriction sites. These sequences were obtained by annealing the following oligonucleotides with protruding single-strand DNA corresponding to the *Nde* I and *Xho* I sites: Antp sense, 5′-TATGGCTCGTCAGATCAAAATCTGGTTCCA GAATCGTCGTATGAAGTGGAAAAAAGGTGGCGGCGGTTC CC-3′; Antp antisense, 5′-TCGAGGGAACCGCCGCCACCTT TTTTCCACTTCATACGACGATTCTGGAACCAGATTTTGATC TGACGAGCCA-3′; Rev sense, 5′-TATGGCTACCCGTCAGGC TCGTCGTAATCGTCGTCGTCGTTGGCGTGAACGTCAGCGT GGTGGCGGCGGTTCCC-3′; Rev antisense, 5′-TCGAGGGAA CCGCCGCCACCACGCTGACGTTCACGCCAACGACGACGA CGATTACGACGAGCCTGACGGGTAGCCA-3′; VP22 sense, 5′-TATGGCTAACGCTAAAACCCGTCGTCACGAACGTCGTCG TAAACTGGCTATCGAACGTGGTGGCGGCGGTTCCC-3′; VP22 antisense, 5′-TCGAGGGAACCGCCGCCACCACGTTCGATAG CCAGTTTACGACGACGTTCGTGACGACGGGTTTTAGCGT TAGCCA-3′. The plasmids, except for the Antp-Venus expression vector, were transformed into *Escherichia coli* BL21 Star (DE3) (Invitrogen). The Antp-Venus-expressing vector was transformed into BL21 Star (DE3), in which the plasmid-expressing chaperone (pGro7) was pretransformed. Transformed *E. coli* was cultured and the cell paste was suspended in BugBuster Master Mix (Novagen, Darmstadt, Germany) and centrifuged. PTD-Venus was recovered in the supernatant and purified by His-tag affinity purification and gel filtration chromatography.

Confocal laser scanning microscopy analysis

HeLa cells were cultured on Lab-Tek II Chambered Coverglass (Nalge Nunc International) at 3.0×10^4 cells per well in MEMα supplemented with 10% FBS and incubated for 24 h at 37 °C. Internalization of PTD-FAM or PTD-Venus was performed as follows: HeLa cells were treated with PTD-FAM or PTD-Venus (10 μM) in Opti-MEM I containing 100 ng ml^{-1} Hoechst 33342 (Invitrogen) and 6 μg ml^{-1} FM4-64 (Invitrogen). After incubation at 37 °C for 3 h, the medium was exchanged with fresh medium and fluorescence was observed by confocal laser scanning microscopy (Leica Microsystems GmbH, Wetzlar, Germany) without cell fixation. For cotreatment with HA2-Tat, HeLa cells were cotreated with PTD-FAM (10 μM) and HA2-Tat (2 μM) in Opti MEM I containing 100 ng ml^{-1} Hoechst 33342. After incubation at 37 °C for 3 h, the medium was exchanged with fresh medium and fluorescence was observed by confocal laser scanning microscopy without cell fixation.

Results

Comparison of transduction efficiency and cytotoxicity of four PTDs

To confirm the intracellular translocation activity of the four selected PTDs, we evaluated the transduction efficiency of Tat-, Antp-, Rev- and VP22-FAM in six cell lines (adherent: HeLa, HaCaT and A431 cells; nonadherent: Jurkat, MOLT-4 and HL60 cells) using flow cytometric analysis (Figure 1). These PTDs contain a large number of basic amino acids (Table 1) and their cationic properties are thought to be important for cell membrane penetration (Futaki *et al.*, 2001; Chauhan *et al.*, 2007). Their positive charge, however, causes them to adsorb nonspecifically to negatively charged cell

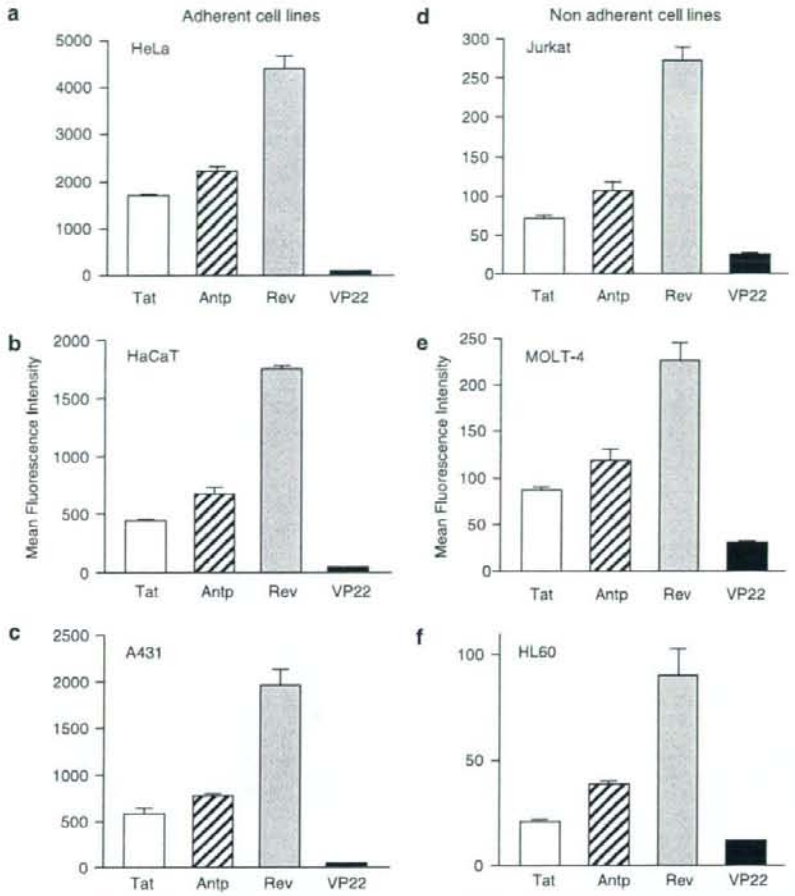

Figure 1 Comparison of the cellular uptake of protein transduction domains (PTDs). FAM-labelled Tat (white column), antennapedia (Antp; hatched column), Rev (grey column) and VP22 (black column) were incubated with six cell lines: HeLa (**a**), HaCaT (**b**), A431 (**c**), Jurkat (**d**), MOLT-4 (**e**) and HL60 (**f**) at 10 μM for 3 h. After trypsin treatment to digest PTDs adsorbed on the cell surface, the PTD-transduced cells were harvested and analysed by flow cytometry. Note that the *y* axis scales for the adherent cell lines are markedly different from that for the nonadherent cell lines. Data shown are the mean ± s.d. of triplicate assays.

membranes (Richard *et al.*, 2003). For this reason, the cells were treated with excess trypsin to eliminate nonspecific plasma membrane binding of the PTDs prior to measurement.

The relative order of their translocation efficiency (Rev > Antp > Tat > VP22), which was based on mean fluorescence, was independent of the cell type (that is, adherent or nonadherent). Furthermore, using PTD-fused Venus, we confirmed that Rev had the highest transduction efficiency (data not shown). Equally important, the overall translocation efficiency of the PTDs depended markedly on whether the cells were adherent (HeLa, HaCaT and A431 cells) or nonadherent (Jurkat, MOLT-4 and HL60 cells). The transduction efficiency was much higher in the adherent cell lines compared with the nonadherent cell lines (Figure 1); note that that the fluorescence (uptake) was about 8- to 25-fold greater in the adherent, than in nonadherent, cell lines.

The cytotoxic properties of the four PTDs were evaluated in adherent (HeLa) and nonadherent (Jurkat) cells. To assess the long-term changes in proliferation, mitochondrial dehydrogenase activity was measured using a WST-8 assay 24 h after PTD treatment. In HeLa cells, there was a remarkable decrease in cell viability when the cells were incubated with Antp at 100 μM, whereas other PTDs were not cytotoxic at the higher concentrations (Figure 2a). In contrast in Jurkat cells, Antp was extremely cytotoxic in a dose-dependent manner and Rev reduced cell proliferation by approximately 40% (Figure 2b). Previous reports indicated that amphipathic peptides, such as transportan, induced cytotoxicity by perturbing the cellular membrane (Hallbrink *et al.*, 2001; Jones *et al.*, 2005; Saar *et al.*, 2005; El-Andaloussi *et al.*, 2007). Thus, the membrane integrity of PTD-treated cells was also measured using an LDH leakage assay. Antp

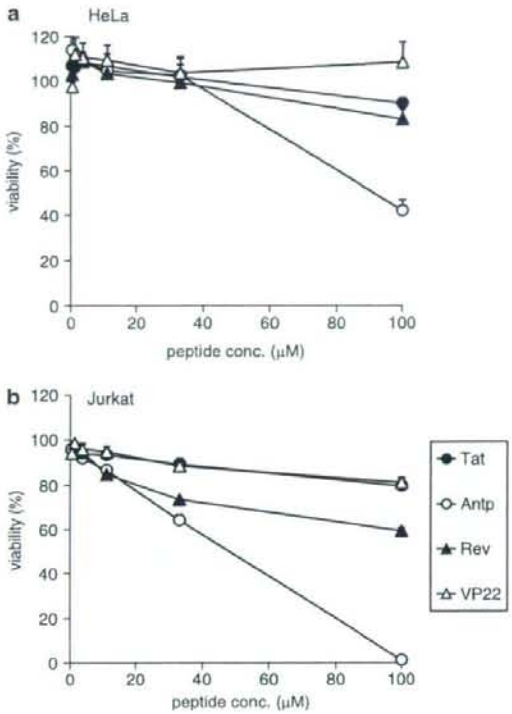

Figure 2 Viability of protein transduction domain (PTD)-treated cells. HeLa cells (**a**) and Jurkat cells (**b**) were incubated with serially diluted biotin-conjugated Tat, antennapedia (Antp), Rev and VP22 at 37 °C. After 24 h, cell viability was analysed using a WST-8 assay. Data shown are the mean ± s.d. of triplicate assays.

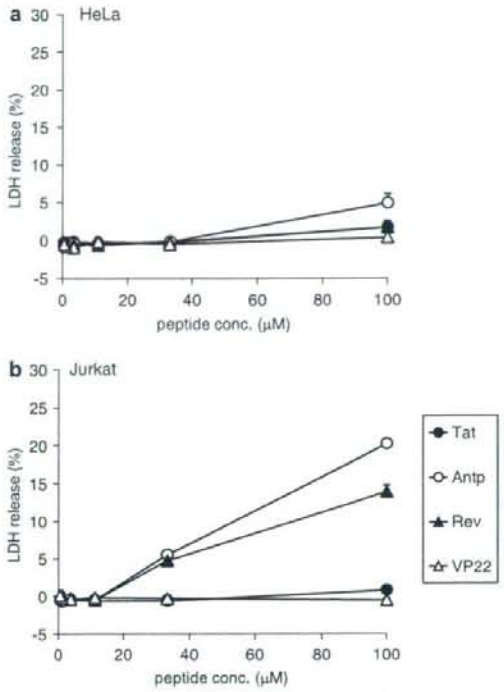

Figure 3 Membrane integrity of protein transduction domain (PTD)-treated cells. HeLa cells (**a**) and Jurkat cells (**b**) were incubated with serially diluted biotin-conjugated Tat, antennapedia (Antp), Rev and VP22 at 37 °C. After 3 h, the release of lactate dehydrogenase (LDH) was analysed. Data shown are the mean ± s.d. of triplicate assays.

and Rev induced significant LDH leakage in Jurkat cells, but only low LDH leakage was detected in Antp-treated HeLa cells (Figure 3). The membrane-perturbing effect of Antp and Rev contributed to the uptake of peptides, which are shown in Figure 1. Jurkat cells appear more sensitive to Antp or Rev treatment than HeLa cells; this difference in cytotoxicity and translocation efficiency may indicate a difference in the PTD-uptake mode.

Intracellular transduction mechanism of PTDs

The results of *in vitro* studies suggest that PTDs enter the cell via an energy-dependent endocytotic pathway (Lundberg *et al.*, 2003; Richard *et al.*, 2003). In particular, studies using various macropinocytosis inhibitors, such as methyl-β-cyclodextrin, to deplete cholesterol from the membrane (Grimmer *et al.*, 2002; Liu *et al.*, 2002), cytochalasin D, to inhibit F-actin elongation (Sampath and Pollard, 1991), or amiloride, to inhibit the Na^+-H^+ exchanger (West *et al.*, 1989), indicate that Tat is taken up into the cell via lipid raft-dependent macropinocytosis. To the best of our knowledge, however, few comparative studies have analysed the cellular uptake pathway of the four PTDs discussed in this paper. Therefore, we used flow cytometry analysis to determine whether PTD uptake is energy dependent or occurs via lipid raft-mediated macropinocytosis. First, we treated cells with PTD-FAM at 37 or 4 °C and then measured cell fluorescence (Figure 4). At 4 °C, transferrin, which enters cells by clathrin-dependent endocytosis (Schmid, 1997), inhibited the transduction efficiency compared with that at 37 °C. All four PTDs had low transduction ability at 4 °C, indicating that their cellular uptake was energy dependent. We next examined the PTD-FAM uptake efficiency in methyl-β-cyclodextrin-, cytochalasin D- and amiloride-treated HeLa cells. These cell treatments inhibited PTD-FAM incorporation in a dose-dependent manner, but transferrin was not affected (Figure 5). Furthermore, in HeLa cells treated with PTD-FAM, only punctuate fluorescence was observed using confocal laser scanning microscopic analysis (Figure 6). These results indicated that all the PTDs evaluated in this study enter the cell through the macropinocytotic pathway and that most of them were trapped in intracellular vesicles, the macropinosomes.

Intracellular localization of PTD–protein conjugates

We next examined the intracellular behaviour of the individual PTDs in more detail. To investigate whether

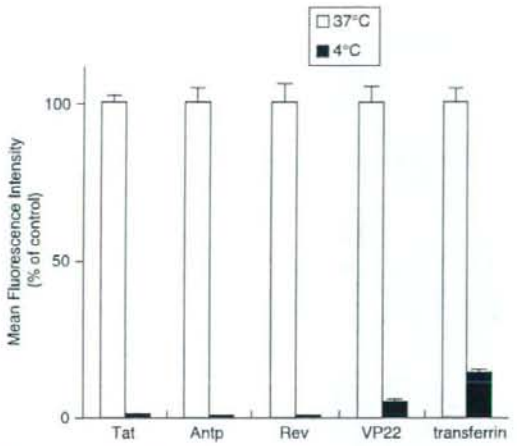

Figure 4 Effects of temperature on protein transduction domain (PTD) transduction efficiency. HeLa cells were preincubated at 37 or 4 °C for 1 h prior to adding FAM-labelled PTDs or fluorescein isothiocyanate-labelled transferrin for 3 h. Cells were washed in trypsin and analysed by flow cytometry. Data shown are the mean ± s.d. of triplicate assays.

individual PTDs are located in the same vesicles, we used Tat-fused HA2 peptide (HA2-Tat), an influenza virus-derived endosome-disrupting peptide. HA2-Tat improves the activity of Tat-fused Cre recombinase (Wadia *et al.*, 2004). Because HA2 alone cannot enter the cell, HA2-Tat is thought to enter the cell in a Tat-dependent manner and to disrupt the membrane of endosomal vesicles in which the Tat cargo is trapped. Thus, if Antp, Rev and VP22 are trapped in the same vesicles as Tat, the fluorescence should spread throughout the cytosol following cotreatment of the cells with HA2-Tat. As predicted, in HeLa cells cotreated with Antp-, Rev- or VP22-Venus and HA2-Tat, the Venus-derived fluorescence spread throughout the cytosol, whereas in the cells treated with Antp-, Rev- or VP22-Venus alone, only punctuate fluorescence was observed (Figure 7). These results suggested that all the PTDs evaluated in this study entered the cell through a macropinocytotic pathway and were trapped in the same vesicles as Tat.

Discussion

In the present study, we have systematically compared PTD-mediated molecular transduction mechanisms. Our findings indicated that individual PTDs have different levels of transduction efficiency and cytotoxicity, suggesting that PTDs are internalized into live cells via different mechanisms. We also examined the internalization pathway and intracellular localization of Tat, Antp, Rev and VP22. Unexpectedly, all the PTDs evaluated in this study entered the cell through the macropinocytotic pathway and were trapped in the same vesicles as Tat. The finding that the intracellular transduction pathways of the four PTDs were the same suggests that the method of cell internalization does not contribute to the

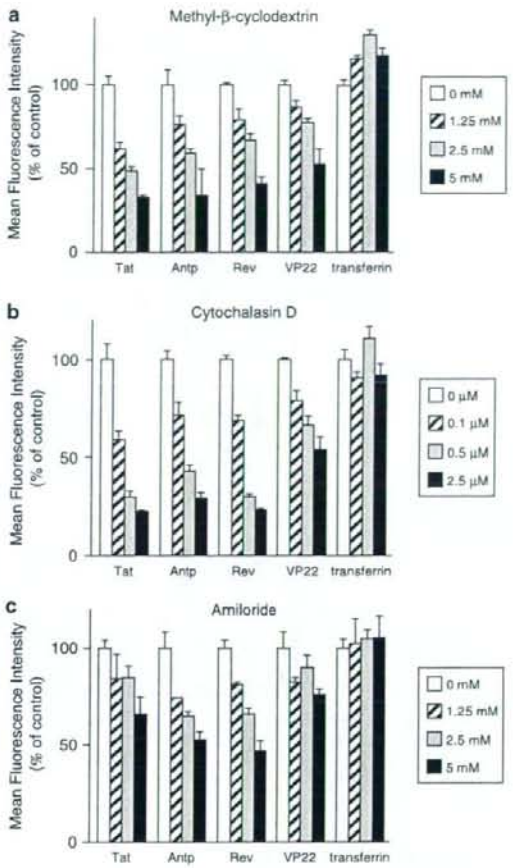

Figure 5 Effects of endocytosis inhibitors on transduction efficiency of protein transduction domains (PTDs). HeLa cells were pretreated with a range of concentrations of (**a**) methyl-β-cyclodextrin, (**b**) cytochalasin D or (**c**) amiloride for 30 min prior to adding FAM-labelled PTDs or fluorescein isothiocyanate-labelled transferrin for 1 h (**a** and **b**) or 30 min (**c**). Cells were washed in trypsin and analysed by flow cytometry. Data shown are the mean ± s.d. of triplicate assays.

differences in the PTD transduction efficiency or cytotoxicity. Although the reason for this phenomenon is not clear, we speculate that the primary structure of the individual PTDs or the cell surface proteins that interact with the individual PTDs contribute to the differences in their transduction efficiency and cytotoxicity.

The initial step in the mechanism of cellular entry of PTDs is thought to be the strong ionic interaction between the amino-acid residues of the PTDs and the plasma membrane constituents. Because the translocation is solely physically mediated, the charge distribution and amphipathicity of the peptide and its interaction with the plasma membrane is critical (Pujals *et al.*, 2006). Although most PTDs, if not all, contain a large number of basic amino acids, such as arginine or lysine, the theoretical isoelectric point (pI) value of each PTD used in this study was essentially identical (Tat, Antp,

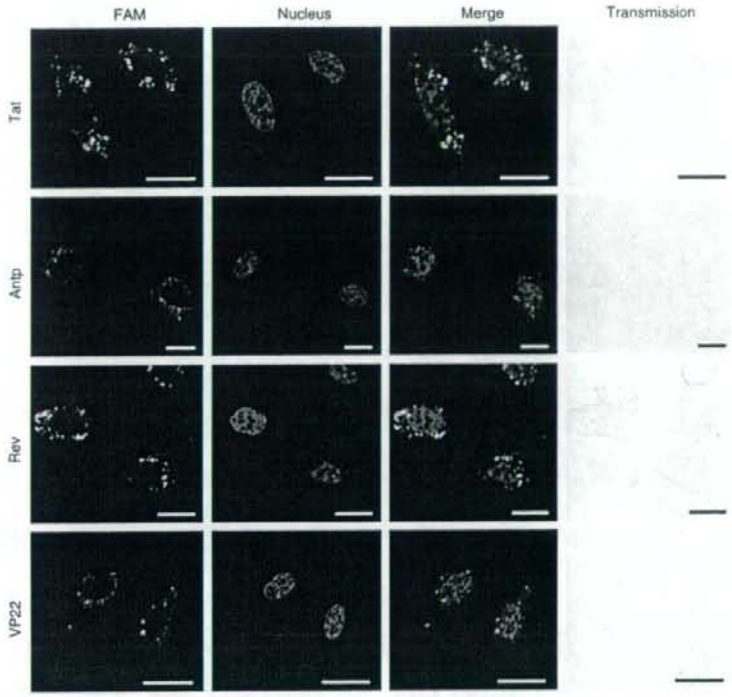

Figure 6 Intracellular behaviour of protein transduction domain (PTD)-FAM in living cells. HeLa cells were treated with 10 μM PTD-FAM for 3 h. Fluorescence images were acquired using confocal laser scanning microscopy and the signals were merged electronically. The nucleus was counterstained with Hoechst 33342 (blue). From top to bottom: Tat-, antennapedia (Antp)-, Rev- and VP22-FAM. From left to right: FAM (green), nucleus (blue), merged fluorescence and transmission image. Scale bars in each microphotograph indicate 20 μm.

Rev and VP22 have pI values of 12.70, 12.31, 12.60 and 12.01, respectively). Therefore, the internalization efficiency does not appear to depend on the cationic features of the PTDs.

The amphipathicity of the carrier is probably responsible not only for the strong interaction with the lipid membranes (Yandek *et al.*, 2007), but also for the disruption of the cellular membrane, which results in cell death (Hallbrink *et al.*, 2001; Jones *et al.*, 2005; Saar *et al.*, 2005; El-Andaloussi *et al.*, 2007). In terms of cytotoxicity, our data indicate that Antp and Rev both disrupt the membrane (Figure 3), but Rev does not contain an amphipathic structure. Furthermore, there was no correlation between hydrophobicity and transduction efficiency. Thus, differences in the PTD-mediated transduction efficiency and cytotoxicity might be due to the molecular weight or pI of the conjugated cargo.

The cellular events required for internalization, however, differ between reports and are often conflicting. The first mechanistic studies led to the proposal that PTD internalization occurs rapidly in a receptor- and energy-independent manner, perhaps by destabilizing the lipid bilayer or by the formation of inverted micelles with subsequent release of their contents within the intracellular space (Berlose *et al.*, 1996). More recently, an active mechanism based on vesicular uptake was proposed as the general mode of cell internalization of PTDs. In our experiment, although all four PTDs tended to be present in the same vesicles, the detailed mechanism for this colocalization is not yet known. It has been suggested that PTD internalization requires cell surface heparan sulphate proteoglycans (Tyagi *et al.*, 2001; Console *et al.*, 2003; Ziegler and Seelig, 2004). Because Tat interacts electrostatically with heparan sulphate proteoglycan present on the cell surface, it is possible that some PTDs are taken into the same vesicles when they interact with one heparan sulphate proteoglycan. In contrast, as shown in Figure 7, although fluorescence was observed throughout the cytosol, punctate fluorescence was also observed when the cells were cotreated with PTD-Venus and HA2-Tat. This finding suggested that the PTDs did not all exist in the same vesicles and that some PTDs entered the cell through another pathway. This is just speculation, however, and we are now using proteome analysis, such as liquid chromatography coupled with mass spectrometry or two-dimensional gel electrophoresis, to examine whether there are individual cell surface receptors for different PTDs.

In summary, our data suggest that Antp, Rev, VP22 and Tat cross the plasma membrane and reach the macropinosomes via different mechanisms. Our findings also indicate that several issues, such as endosome entrapment and low cell specificity, which limit the therapeutic activity of the cargo,

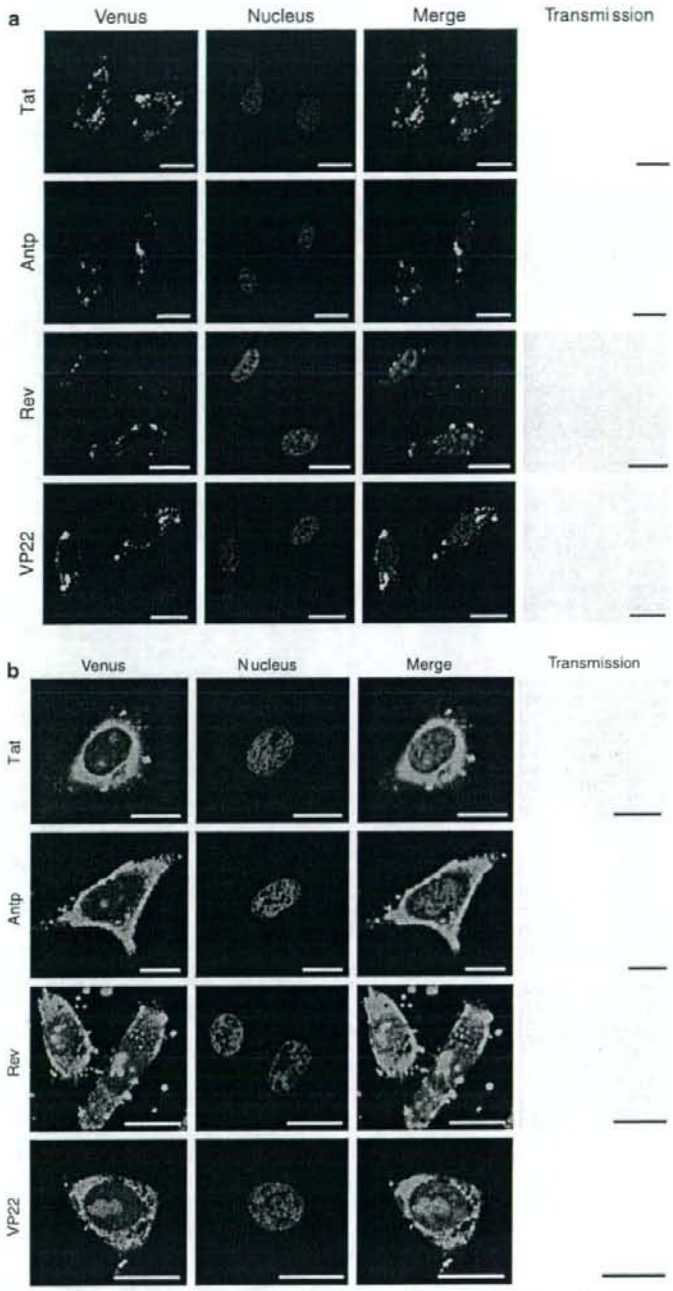

Figure 7 Intracellular behaviour of protein transduction domain (PTD)-Venus in living cells. HeLa cells were treated with 10 μM PTD-Venus alone (**a**) or 10 μM HA2-Tat (**b**) for 3 h. Fluorescence images were acquired using confocal laser scanning microscopy and the signals were merged electronically. The nucleus was counterstained with Hoechst 33342 (blue). From top to bottom: Tat-, antennapedia (Antp)-, Rev- and VP22-Venus. From left to right: Venus (green), nucleus (blue), merged fluorescence and transmission image. Scale bars in each microphotograph indicate 20 μm.

must be overcome before effective PTD-based drug delivery carriers can be fully developed. We previously reported that cotreatment with HA2-Tat enhances the cytosolic release of Tat-fused peptide-blockers and their biological activities, thereby overcoming the issue of endosome entrapment (Sugita *et al.*, 2007). Furthermore, although the transduction mechanism of PTDs is not yet well understood, these differences led us to explore the possibility of creating novel PTDs. We successfully created novel PTDs that have higher transduction efficiencies than Tat, using a unique phage display-based screening strategy that we previously developed (Mukai *et al.*, 2006; Kamada *et al.*, 2007). Moreover, based on our PTD-screening system, we are currently working to create more useful PTDs with cell type specificity.

Conflict of interest

The authors state no conflict of interest.

References

Berlose JP, Convert O, Derossi D, Brunissen A, Chassaing G (1996). Conformational and associative behaviours of the third helix of antennapedia homeodomain in membrane-mimetic environments. *Eur J Biochem* **242**: 372–386.

Borsello T, Forloni G (2007). JNK signalling: a possible target to prevent neurodegeneration. *Curr Pharm Des* **13**: 1875–1886.

Brusic V, Marina O, Wu CJ, Reinherz EL (2007). Proteome informatics for cancer research: from molecules to clinic. *Proteomics* **7**: 976–991.

Chauhan A, Tikoo A, Kapur AK, Singh M (2007). The taming of the cell penetrating domain of the HIV Tat: myths and realities. *J Control Release* **117**: 148–162.

Console S, Marty C, Garcia-Echeverria C, Schwendener R, Ballmer-Hofer K (2003). Antennapedia and HIV transactivator of transcription (TAT) 'protein transduction domains' promote endocytosis of high molecular weight cargo upon binding to cell surface glycosaminoglycans. *J Biol Chem* **278**: 35109–35114.

Derossi D, Joliot AH, Chassaing G, Prochiantz A (1994). The third helix of the Antennapedia homeodomain translocates through biological membranes. *J Biol Chem* **269**: 10444–10450.

Drabik A, Bierczynska-Krzysik A, Bodzon-Kulakowska A, Suder P, Kotlinska J, Silberring J (2007). Proteomics in neurosciences. *Mass Spectrom Rev* **26**: 432–450.

El-Andaloussi S, Jarver P, Johansson HJ, Langel U (2007). Cargo dependent cytotoxicity and delivery efficacy of cell-penetrating peptides: a comparative study. *Biochem J* **407**: 285–292.

Elliott G, O'Hare P (1997). Intercellular trafficking and protein delivery by a herpesvirus structural protein. *Cell* **88**: 223–233.

Ferrari A, Pellegrini V, Arcangeli C, Fittipaldi A, Giacca M, Beltram F (2003). Caveolae-mediated internalization of extracellular HIV-1 tat fusion proteins visualized in real time. *Mol Ther* **8**: 284–294.

Fittipaldi A, Ferrari A, Zoppe M, Arcangeli C, Pellegrini V, Beltram F *et al.* (2003). Cell membrane lipid rafts mediate caveolar endocytosis of HIV-1 Tat fusion proteins. *J Biol Chem* **278**: 34141–34149.

Futaki S, Suzuki T, Ohashi W, Yagami T, Tanaka S, Ueda K *et al.* (2001). Arginine-rich peptides. An abundant source of membrane-permeable peptides having potential as carriers for intracellular protein delivery. *J Biol Chem* **276**: 5836–5840.

Grimmer S, van Deurs B, Sandvig K (2002). Membrane ruffling and macropinocytosis in A431 cells require cholesterol. *J Cell Sci* **115**: 2953–2962.

Hallbrink M, Floren A, Elmquist A, Pooga M, Bartfai T, Langel U (2001). Cargo delivery kinetics of cell-penetrating peptides. *Biochim Biophys Acta* **1515**: 101–109.

Han X, Bushweller JH, Cafiso DS, Tamm LK (2001). Membrane structure and fusion-triggering conformational change of the fusion domain from influenza hemagglutinin. *Nat Struct Biol* **8**: 715–720.

Hawiger J (1999). Noninvasive intracellular delivery of functional peptides and proteins. *Curr Opin Chem Biol* **3**: 89–94.

Joliot A, Prochiantz A (2004). Transduction peptides: from technology to physiology. *Nat Cell Biol* **6**: 189–196.

Jones SW, Christison R, Bundell K, Voyce CJ, Brockbank SM, Newham P *et al.* (2005). Characterisation of cell-penetrating peptide-mediated peptide delivery. *Br J Pharmacol* **145**: 1093–1102.

Kamada H, Okamoto T, Kawamura M, Shibata H, Abe Y, Ohkawa A *et al.* (2007). Creation of novel cell-penetrating peptides for intracellular drug delivery using systematic phage display technology originated from Tat transduction domain. *Biol Pharm Bull* **30**: 218–223.

Kaplan IM, Wadia JS, Dowdy SF (2005). Cationic TAT peptide transduction domain enters cells by macropinocytosis. *J Control Release* **102**: 247–253.

Liu NQ, Lossinsky AS, Popik W, Li X, Gujuluva C, Kriederman B *et al.* (2002). Human immunodeficiency virus type 1 enters brain microvascular endothelia by macropinocytosis dependent on lipid rafts and the mitogen-activated protein kinase signaling pathway. *J Virol* **76**: 6689–6700.

Lundberg M, Wikstrom S, Johansson M (2003). Cell surface adherence and endocytosis of protein transduction domains. *Mol Ther* **8**: 143–150.

Mukai Y, Sugita T, Yamato T, Yamanada N, Shibata H, Imai S *et al.* (2006). Creation of novel protein transduction domain (PTD) mutants by a phage display-based high-throughput screening system. *Biol Pharm Bull* **29**: 1570–1574.

Murriel CL, Dowdy SF (2006). Influence of protein transduction domains on intracellular delivery of macromolecules. *Expert Opin Drug Deliv* **3**: 739–746.

Nagahara H, Vocero-Akbani AM, Snyder EL, Ho A, Latham DG, Lissy NA *et al.* (1998). Transduction of full-length TAT fusion proteins into mammalian cells: TAT-p27Kip1 induces cell migration. *Nat Med* **4**: 1449–1452.

Nori A, Kopecek J (2005). Intracellular targeting of polymer-bound drugs for cancer chemotherapy. *Adv Drug Deliv Rev* **57**: 609–636.

Pujals S, Fernandez-Carneado J, Lopez-Iglesias C, Kogan MJ, Giralt E (2006). Mechanistic aspects of CPP-mediated intracellular drug delivery: relevance of CPP self-assembly. *Biochim Biophys Acta* **1758**: 264–279.

Rhodes DR, Chinnaiyan AM (2005). Integrative analysis of the cancer transcriptome. *Nat Genet* **37** (Suppl): S31–S37.

Richard JP, Melikov K, Brooks H, Prevot P, Lebleu B, Chernomordik LV (2005). Cellular uptake of unconjugated TAT peptide involves clathrin-dependent endocytosis and heparan sulfate receptors. *J Biol Chem* **280**: 15300–15306.

Richard JP, Melikov K, Vives E, Ramos C, Verbeure B, Gait MJ *et al.* (2003). Cell-penetrating peptides. A reevaluation of the mechanism of cellular uptake. *J Biol Chem* **278**: 585–590.

Rojas M, Donahue JP, Tan Z, Lin YZ (1998). Genetic engineering of proteins with cell membrane permeability. *Nat Biotechnol* **16**: 370–375.

Saar K, Lindgren M, Hansen M, Eiriksdottir E, Jiang Y, Rosenthal-Aizman K *et al.* (2005). Cell-penetrating peptides: a comparative membrane toxicity study. *Anal Biochem* **345**: 55–65.

Sampath P, Pollard TD (1991). Effects of cytochalasin, phalloidin, and pH on the elongation of actin filaments. *Biochemistry* **30**: 1973–1980.

Schmid SL (1997). Clathrin-coated vesicle formation and protein sorting: an integrated process. *Annu Rev Biochem* **66**: 511–548.

Schwarze SR, Ho A, Vocero-Akbani A, Dowdy SF (1999). *In vivo* protein transduction: delivery of a biologically active protein into the mouse. *Science* **285**: 1569–1572.

Schwarze SR, Hruska KA, Dowdy SF (2000). Protein transduction: unrestricted delivery into all cells? *Trends Cell Biol* **10**: 290–295.

Skehel JJ, Cross K, Steinhauer D, Wiley DC (2001). Influenza fusion peptides. *Biochem Soc Trans* **29**: 623–626.

Sugita T, Yoshikawa T, Mukai Y, Yamanada N, Imai S, Nagano K *et al.* (2007). Improved cytosolic translocation and tumor-killing

activity of Tat-shepherdin conjugates mediated by co-treatment with Tat-fused endosome-disruptive HA2 peptide. *Biochem Biophys Res Commun* **363**: 1027–1032.

Tyagi M, Rusnati M, Presta M, Giacca M (2001). Internalization of HIV-1 tat requires cell surface heparan sulfate proteoglycans. *J Biol Chem* **276**: 3254–3261.

Wadia JS, Stan RV, Dowdy SF (2004). Transducible TAT-HA fusogenic peptide enhances escape of TAT-fusion proteins after lipid raft macropinocytosis. *Nat Med* **10**: 310–315.

West MA, Bretscher MS, Watts C (1989). Distinct endocytotic pathways in epidermal growth factor-stimulated human carcinoma A431 cells. *J Cell Biol* **109**: 2731–2739.

Yandek LE, Pokorny A, Floren A, Knoelke K, Langel U, Almeida PF (2007). Mechanism of the cell-penetrating peptide transportan 10 permeation of lipid bilayers. *Biophys J* **92**: 2434–2444.

Ziegler A, Seelig J (2004). Interaction of the protein transduction domain of HIV-1 TAT with heparan sulfate: binding mechanism and thermodynamic parameters. *Biophys J* **86**: 254–263.

doi:10.1016/j.jmb.2008.05.047 J. Mol. Biol. (2008) 380, 777–782

JMB

Available online at www.sciencedirect.com

ScienceDirect

ELSEVIER

COMMUNICATION

Organelle-Targeted Delivery of Biological Macromolecules Using the Protein Transduction Domain: Potential Applications for Peptide Aptamer Delivery into the Nucleus

Tomoaki Yoshikawa[1,2]†, Toshiki Sugita[1,2]†, Yohei Mukai[1,2], Natsue Yamanada[1,2], Kazuya Nagano[1,2], Hiromi Nabeshi[1,2], Yasuo Yoshioka[1,3], Shinsaku Nakagawa[2], Yasuhiro Abe[1], Haruhiko Kamada[1,3], Shin-ichi Tsunoda[1,3]* and Yasuo Tsutsumi[1,2,3]

[1]*Laboratory of Pharmaceutical Proteomics, National Institute of Biomedical Innovation, 7-6-8 Saito-Asagi, Ibaraki, Osaka 567-0085, Japan*

[2]*Graduate School of Pharmaceutical Sciences, Osaka University, 1-6 Yamadaoka, Suita, Osaka 565-0871, Japan*

[3]*The Center for Advanced Medical Engineering and Informatics, Osaka University, 1-6 Yamadaoka, Suita, Osaka 565-0871, Japan*

Received 5 March 2008; received in revised form 16 May 2008; accepted 21 May 2008
Available online 29 May 2008

Edited by J. Karn

Extensive effort is currently being expended on the innovative design and engineering of new molecular carrier systems for the organelle-targeted delivery of biological cargoes (e.g., peptide aptamers or biological proteins) as tools in cell biology and for developing novel therapeutic approaches. Although cell-permeable Tat peptides are useful carriers for delivering biological molecules into the cell, much internalized Tat-fused cargo is trapped within macropinosomes and thus not delivered into organelles. Here, we devised a novel intracellular targeting technique to deliver Tat-fused cargo into the nucleus using an endosome-disruptive peptide (hemagglutinin-2 subunit) and a nuclear localization signal peptide. We show for the first time that Tat-conjugated peptide aptamers can be selectively delivered to the nucleus by using combined hemagglutinin-2 subunit and nuclear localization signal peptides. This nuclear targeting technique resulted in marked enhancement of the cytostatic activity of a Tat-fused p53-derived peptide aptamer against human MDM2 (mouse double minute 2) that inhibits p53–MDM2 binding. Thus, our technique provides a unique methodology for the development of novel therapeutic approaches based on intracellular targeting.

Keywords: Tat; HA2; nuclear localization signal; intracellular targeting; peptide aptamer

Progress in molecular biological research on intractable diseases such as cancer is steadily increasing our knowledge of the mechanisms of malignant transformation occurring in tumor cells. However, the complexity of biological interactions makes it increasingly difficult to predict gene and protein functions as we proceed from the immediate metabolic pathway to the levels of the cell and organism. Especially at the cellular level, a variety of tools are available to determine protein function and to develop novel therapeutic approaches, including antisense, peptide modulators, proteins and the overexpression of wild-type or dominant-negative proteins. Small peptides might be able to complement these agents because of

T.S. and T.Y. contributed equally to this work.

*Corresponding author. Laboratory of Pharmaceutical Proteomics, National Institute of Biomedical Innovation, 7-6-8 Saito-Asagi, Ibaraki, Osaka 567-0085, Japan. E-mail address: tsunoda@nibio.go.jp.

† T.S. and T.Y. contributed equally to this work.

Abbreviations used: MDM2, mouse double minute 2; PTD, protein transduction domain; HA2, hemagglutinin-2 subunit; NLS, nuclear localization signal; NLS–VENUS–Tat, VENUS protein with Tat, NLS and His tag; Tat–cargo, Tat-fused cargo; HA2–Tat, Tat-fused endosome-disruptive HA2 peptide; PM10–Tat, Tat-fused PM10; NLS–PM10–

their ability to recognize specific protein domains and thus to interfere with enzymatic functions or protein–protein interactions.[1] Furthermore, these peptides, designated "peptide aptamers," seem to be non-genotoxic and useful for adjunct chemotherapy. However, these approaches are often limited by an inability to effectively deliver the agents to the appropriate cellular location.

Because a prerequisite for their intracellular action is their delivery into cells, various intracellular delivery approaches, such as protein transduction technology with protein transduction domains (PTDs; e.g., Tat, Antp, VP22, Rev and so on), are currently undergoing intensive scrutiny.[2,3] However, protein transduction technology using PTDs has some disadvantages, one of which is the accumulation of PTDs or PTD-fused peptides in the endocytic compartment. We and others have reported that the main mechanism of protein transduction is penetration into cells by macropinocytosis and that therefore much of the material taken up remains entrapped in the macropinosomes.[4–7] Another disadvantage is that there is no technique for controlling the intracellular distribution of peptide aptamers such that their effects are extremely limited. For these reasons, it is important that peptide aptamers be delivered directly into specific cellular compartments. Because optimal approaches for overcoming these disadvantages have not yet been developed, high concentrations of PTDs or PTD-fused peptides must still be employed in order for the technology to function effectively.

With this in mind, we focused on developing intracellular targeting technology for peptide aptamers fused with Tat protein basic domain residues 47–57 (YGRKKRRQRRR) from human immunodeficiency virus-1 in the context of cancer therapeutics. We recently reported that survivin-targeted peptide aptamers (shepherdin) linked to the NH_2-terminal domain of the influenza virus hemagglutinin-2 subunit (HA2), which is a pH-dependent fusogenic peptide inducing lysis of membranes at low pH levels,[8,9] are efficiently released from macropinosomes. This approach succeeded in inducing the death of survivin-expressing malignant tumor cells.[10] Based on this previous study, here we devised a novel intracellular targeting technology using HA2 and nuclear localization signal (NLS) peptides for converting peptide aptamers into efficient research tools for cell biology and cancer therapeutics. We established for the first time that Tat-conjugated peptide aptamers can be selectively delivered to the nucleus by combining HA2 and NLS peptides. Furthermore, we evaluated the utility of our nuclear targeting method using p53-derived peptide from the human MDM2 (mouse double minute 2, also termed HDM2 in humans)-binding domain (residues 17–26: designated PM10), which is a peptide inhibitor of p53–MDM2 binding.[11] Recent reports suggested that inhibiting p53–MDM2 binding could reactivate the p53 pathway and induce growth-suppressive effects and cell cycle arrest of tumor cells as well as normal cells possessing wild-type p53.[11–17] Because the interaction of p53 and MDM2 takes place inside the nucleus, nuclear delivery of PM10 may potentiate the cytostatic effect of this agent. Indeed, we found that our nuclear targeting technique employing PTD, HA2 and NLS peptides markedly enhanced PM10-mediated cytostatic effects against A549 (human lung adenocarcinoma) and WI-38 (human embryonic fibroblast, lung-derived cell line) cells. These results indicate that our intracellular targeting techniques can deliver the cargo into the appropriate organelle and provide a unique research tool for cellular biology and the development of novel therapeutic approaches.

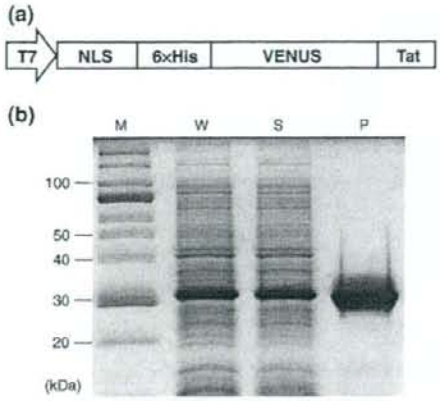

Fig. 1. Vector construction and SDS-PAGE analysis of NLS–VENUS–Tat. (a) Schematic of the NLS–VENUS–Tat region of T7 promoter-driven protein expression vector. The VENUS (variant of yellow fluorescent protein) DNA sequence was kindly provided by Dr. A. Miyawaki (RIKEN Brain Science Institute, Saitama, Japan). The NLS–VENUS–Tat DNA sequence was amplified by PCR. At the 5′ end, the primer sequence 5′-AA CTT TAA GAA GGA GAT ATA *CAT ATG* CCG AAA AAG AAA CGT AAA GTT ACC ATG GCT CAC CAC CAT CAC CAC CAT **GAC TAC AAA GAC GAT GAT GAC AAA** GAA GCT TAC GTG AGC AAG GGC GAG GAG CTG TT-3′ introduced an NdeI site (italics), an NLS (boldface) and a 6× His tag (underline); at the 3′ end, the primer sequence 5′-T TCC TTT CGG GCT TTG TTA GCA GCC *GAA TTC* TTA TTA **ACG GCG ACG CTG GCG ACG TTT TTT ACG ACC GTA** CTC GAG CTT GTA CAG CTC GTC CAT GCC GAG-3′ introduced an EcoRI site (italics) and a Tat sequence (boldface). The PCR product was digested with NdeI as well as EcoRI and inserted into pT7 vector, under the control of the T7 promoter. (b) The plasmid was transformed into *E. coli* BL21 Star (DE3) (Invitrogen, Carlsbad, CA), and cells expressing VENUS proteins were cultured at 25 °C, 250 rpm, for 6 h. The cell paste was then solubilized in a BugBuster Master Mix (Novagen, Darmstadt, Germany) and centrifuged. NLS–VENUS–Tat was recovered in the supernatant and purified by His-tag affinity purification and gel-filtration chromatography. SDS-PAGE analysis was performed under reducing conditions. Lane M, molecular weight standard; lane W, *E. coli* extracts prepared after induction of expression by IPTG; lane S, soluble fractions; lane P, purified proteins.

Tat-fused cargo can be selectively delivered to the nucleus by combining HA2 and NLS peptides

We constructed a VENUS protein (variant of yellow fluorescent protein) fused with Tat, NLS and His tag (NLS–VENUS–Tat) for use as an expression vector (Fig. 1a). NLS–VENUS–Tat was indeed expressed in *Escherichia coli* [BL21 Star (DE3)] after induction with IPTG. The level of expression of the NLS–VENUS–Tat protein was analyzed by SDS-PAGE in total cell lysates (Fig. 1b). Protein expression was specifically induced because we did not find substantially leaky expression of the recombinant protein (data not shown). Recombinant NLS–VENUS–Tat was produced almost entirely in the soluble fraction and had an apparent molecular mass of about 32 kDa under reducing conditions (Fig. 1b, lane S). Purification was carried out by lysis, and separation of the soluble fraction was carried out by centrifugation. This was then loaded onto a Ni^{2+} column for initial purification. The NLS–VENUS–Tat protein eluted from the Ni^{2+} column was more than 90% pure (Fig. 1b, lane P). The purity, apparent molecular mass and cellular internalization activity of the eluted NLS–VENUS–Tat proteins were established by SDS-PAGE and flow cytometry.

Numerous mechanistic studies have shown that Tat peptides rapidly permeate plasma membranes and translocate into the nucleus.[18–22] This mechanism is currently used to deliver proteins and nucleic acids to cell nuclei through covalent linkages of Tat and cargoes.[18] However, nuclear delivery has remained problematic and very limited, because endosome escape and nuclear transport of Tat-fused cargo (Tat–cargo) represent a passive rather than an active process. Indeed, in HeLa cells treated with NLS–VENUS–Tat alone, only punctate cytoplasmic fluorescence, and no fluorescence in the nucleus, was observed (Fig. 2). We had previously confirmed that Tat-fused VENUS co-localized in live cells to vesicles with FM4-64, which is a general endosome marker (data not shown). Furthermore, FAM (carboxyfluorescein) dye-fused Tat peptides also co-localized in FM4-64-positive endosomal vesicles (data not shown). Thus, these results indicated that much of the NLS–VENUS–Tat was entrapped within the endosomal vesicles, resulting in low levels of nuclear accumulation. It is therefore reasonable to propose that Tat–cargo alone cannot reach the targeted cellular compartment, especially the nucleus, and that the therapeutic effects of anticancer peptide aptamers are extremely limited for this reason. Therefore, we devised an active nuclear targeting technique using endosome-disruptive HA2 and SV40-derived NLS peptides.

Recently, we reported that co-treatment with Tat–cargo and the Tat-fused endosome-disruptive HA2 peptide (HA2–Tat) improved the endosome-escape ability and the tumor-killing activity of Tat-fused antisurvivin peptide aptamers.[10] Therefore, we hypothesized that NLS–VENUS–Tat can be delivered into the nucleus if NLS–VENUS–Tat can be engineered to escape from the endosomal vesicles into the cytosol by co-treatment with HA2–Tat. To investigate whether co-treatment with HA2–Tat does effectively improve the nuclear localization of NLS–Tat–cargo, we co-treated HeLa cells with NLS–VENUS–Tat and HA2–Tat and analyzed the intracellular localization of NLS–VENUS–Tat by confocal laser scanning

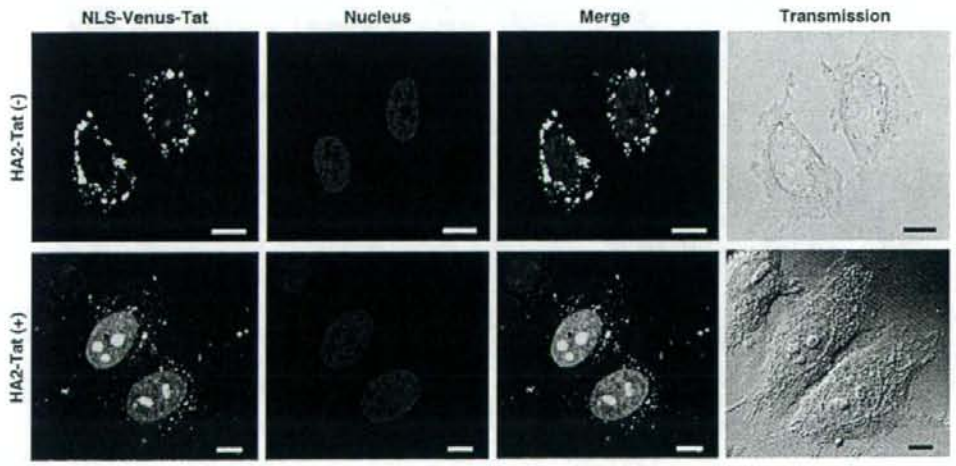

Fig. 2. Intracellular distribution of NLS–VENUS–Tat. HeLa cells were cultured on a Lab-Tek II Chambered Coverglass system (Nalge Nunc International) at 3.0×10^4 cells/well in MEM (minimum essential medium)-α supplemented with 10% fetal bovine serum and incubated for 24 h at 37 °C. Internalization of NLS–VENUS–Tat was performed as follows: HeLa cells were co-treated with NLS–VENUS–Tat (10 μM) with or without HA2–Tat (5 μM) in Opti-MEM I (Invitrogen) containing 100 ng/ml of Hoechst 33342 (Invitrogen). After incubation at 37 °C for 3 h, the medium was changed for a fresh medium and assessed by confocal laser scanning microscopy (Leica Microsystems GmbH, Wetzlar, Germany) without cell fixation. Scale bars in each photomicrograph represent 10 μm.

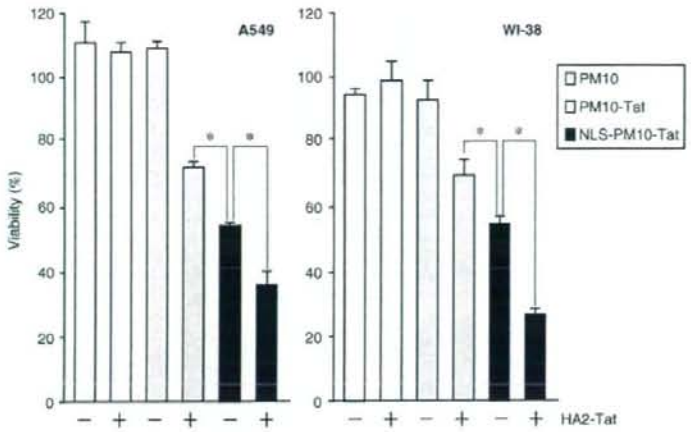

Fig. 3. Nuclear targeting potentiates the cytostatic effect of PM10. All peptides used in this study were purchased from GL Biochem Ltd. (Hiroshima, Japan) with confirmed purities >90% by HPLC and mass spectrography. The sequences of these peptides were GLFEAIEGFIENGWEGMIDGWYG**YGRKKRRQRRR** for HA2–Tat, ETFSDLWKLL for PM10, ETFSDLWKLL**YGRKKRRQRRR** for PM10–Tat and PKKKRKVETFSDLWKLL**YGRKKRRQRRR** for NLS–PM10–Tat. Tat and NLS are shown in boldface and underlined, respectively. A549 or WI-38 cells were seeded into 96-well tissue culture plates (Nalge Nunc International) at 1.0×10^4 cells/well. After incubation for 24 h at 37 °C, the cells were treated with PM10, PM10–Tat or NLS–PM10–Tat at 6 μM (for A549 cells) or 12 μM (for WI-38 cells) in the presence or absence of HA2–Tat (5 μM). After 6 h (for A549 cells) or 24 h (for WI-38 cells), cell viability was determined with the use of WST-8 assay (Nakalai Tesque Inc., Kyoto, Japan) according to the manufacturer's protocol. Data are presented as the mean±SD of triplicate assays. Statistical treatment of the data was performed according to Student's *t* test for two populations (*$p<0.01$).

microscopy (Fig. 2). Co-treatment of HeLa cells with NLS–VENUS–Tat and HA2–Tat resulted in nuclear localization of VENUS, co-localized with Hoechst 33342-stained nuclei. This finding documents that Tat–cargo can be selectively delivered to the nucleus by using HA2 and NLS peptides. Although several groups have attempted to deliver macromolecular drugs to specific organelles, they used PTDs conjugated only with an organelle-targeting signal, such as NLS or mitochondria-targeting signal.[23,24,25] Our data revealed that NLS–VENUS–Tat was entrapped within the endosomal vesicles, with no detectable fluorescence derived from VENUS found in the nucleus. This indicates that organelle targeting by signal-fused PTD–cargo alone does not allow efficient migration into the targeted organelle in the absence of an endosome-escape strategy. Although the influence of the use of different cell types, fluorescent dye, cargo, incubation time and so on could not be excluded as contributing to targeting inability, we found that nuclear transport efficiency could be augmented by combining PTD, HA2 and NLS peptides. Furthermore, our results imply that macromolecules could be delivered into other organelles, such as mitochondria, endoplasmic reticulum and peroxisomes, using different organelle-targeting signal sequences. To this end, we are currently developing novel intracellular drug delivery systems that can target macromolecules into different organelles in a manner analogous to our nuclear targeting techniques.

Nuclear targeting enhances the cytostatic activity of anti-MDM2 peptide aptamer

Next, we tested the utility of our nuclear targeting method using the MDM2-binding peptide aptamer, PM10, which is a p53-derived peptide corresponding to a sequence within the MDM2-binding domain. Kanovsky *et al.* reported that PTD-mediated intracellular delivery of PM10 could reactivate p53 and induce p53-mediated apoptosis of tumor cells with wild-type p53.[11] Under physiological conditions, growth-suppressive and proapoptotic activity of p53 is inhibited by MDM2, which binds p53 and negatively regulates its activity and stability.[16] Recent reports indicated that prevention of p53–MDM2 binding activates the p53 signaling pathway and induces p53-dependent apoptosis in cancer cells possessing wild-type p53.[12,14,15] In addition, the abrogation of p53–MDM2 binding mediates a cytostatic effect and cell cycle arrest in proliferating normal cells.[13,15,17] Because PM10 seems to bind nuclear-localized MDM2 and inhibits MDM2-inducible ubiquitination and degradation of p53, we hypothesized that the nuclear targeting method using HA2 and NLS peptides would enhance its cytotoxicity. To test this, we investigated the effects of treatment with PM10 on cell viability using A549 (human lung adenocarcinoma) and WI-38 (human lung-derived embryonic fibroblast) cells, which possess wild-type p53 (Fig. 3). In A549 and WI-38 cells treated with PM10, Tat-fused PM10 (PM10–Tat) grew vigorously. However, co-treatment with HA2–Tat and PM10–Tat together markedly inhibited A549 and WI-38 cell growth. Furthermore, A549 and WI-38 cells co-treated with HA2–Tat and NLS-fused PM10–Tat (NLS–PM10–Tat) showed greater growth inhibition compared with those treated with NLS–PM10–Tat alone. According to a report from the developers of PM10, although transduction of PTD-fused PM10 (PM10-PTD) into cancer cells could induce tumor cell death *in vitro* and *in vivo*, a high concentration of PM10-PTD was required to see an effect on cancer

cells.[11,26] In contrast, our nuclear targeting technique using PTD, HA2 and NLS peptides markedly enhanced the nuclear localization of the cargo and the PM10-mediated cytostatic effect at low concentrations of PM10. To the best of our knowledge, this is the first report that nuclear targeting of MDM2-binding peptide aptamers can lead to augmentation of cytostatic activity.

In the present study, we aimed to develop a novel cancer therapeutic approach by controlling apoptotic pathways using peptide-based drugs. Recently, the use of intracellular antibodies (intrabodies) directed to a specific target antigen present in the cell has also been suggested as a therapeutic lead to control the apoptotic pathway.[27,28] Our organelle-targeting strategy does seem able to deliver intrabodies directly to the specific organelle in which disease-related proteins reside. Furthermore, we have generated antibodies for various targeted antigens using a non-immune phage scFv library.[29] Thus, we are also currently developing a novel approach to intracellular therapy combining an organelle-targeting strategy and antibody engineering.

Acknowledgements

This study was supported in part by Grants-in-Aid for Scientific Research (20790156) from the Ministry of Education, Culture, Sports, Science and Technology of Japan; in part by a Health and Labor Sciences Research Grant from the Ministry of Health, Labor and Welfare of Japan; in part by a Grant for Industrial Technology Research Program (03A47016a) from the New Energy and Industrial Technology Development Organization of Japan; and in part by funding from the Takeda Science Foundation.

References

1. Mendoza, F. J., Espino, P. S., Cann, K. L., Bristow, N., McCrea, K. & Los, M. (2005). Anti-tumor chemotherapy utilizing peptide-based approaches—apoptotic pathways, kinases, and proteasome as targets. *Arch. Immunol. Ther. Exp.* **53**, 47–60.
2. Dietz, G. P. & Bahr, M. (2004). Delivery of bioactive molecules into the cell: the Trojan horse approach. *Mol. Cell. Neurosci.* **27**, 85–131.
3. Chauhan, A., Tikoo, A., Kapur, A. K. & Singh, M. (2007). The taming of the cell penetrating domain of the HIV Tat: myths and realities. *J. Controlled Release*, **117**, 148–162.
4. Fretz, M., Jin, J., Conibere, R., Penning, N. A., Al-Taei, S., Storm, G. *et al.* (2006). Effects of Na^+/H^+ exchanger inhibitors on subcellular localisation of endocytic organelles and intracellular dynamics of protein transduction domains HIV-TAT peptide and octaarginine. *J. Controlled Release*, **116**, 247–254.
5. Wadia, J. S., Stan, R. V. & Dowdy, S. F. (2004). Transducible TAT-HA fusogenic peptide enhances escape of TAT-fusion proteins after lipid raft macropinocytosis. *Nat. Med.* **10**, 310–315.
6. Sugita, T., Yoshikawa, T., Mukai, Y., Yamanada, N., Imai, S., Nagano, K. *et al.* (2008). Comparative study on transduction and toxicity of protein transduction domains. *Br. J. Pharmacol.* **153**, 1143–1152.
7. Kaplan, I. M., Wadia, J. S. & Dowdy, S. F. (2005). Cationic TAT peptide transduction domain enters cells by macropinocytosis. *J. Controlled Release*, **102**, 247–253.
8. Han, X., Bushweller, J. H., Cafiso, D. S. & Tamm, L. K. (2001). Membrane structure and fusion-triggering conformational change of the fusion domain from influenza hemagglutinin. *Nat. Struct. Biol.* **8**, 715–720.
9. Skehel, J. J., Cross, K., Steinhauer, D. & Wiley, D. C. (2001). Influenza fusion peptides. *Biochem. Soc. Trans.* **29**, 623–626.
10. Sugita, T., Yoshikawa, T., Mukai, Y., Yamanada, N., Imai, S., Nagano, K. *et al.* (2007). Improved cytosolic translocation and tumor-killing activity of Tat-shepherdin conjugates mediated by co-treatment with Tat-fused endosome-disruptive HA2 peptide. *Biochem. Biophys. Res. Commun.* **363**, 1027–1032.
11. Kanovsky, M., Raffo, A., Drew, L., Rosal, R., Do, T., Friedman, F. K. *et al.* (2001). Peptides from the amino terminal mdm-2-binding domain of p53, designed from conformational analysis, are selectively cytotoxic to transformed cells. *Proc. Natl. Acad. Sci. USA*, **98**, 12438–12443.
12. Vassilev, L. T., Vu, B. T., Graves, B., Carvajal, D., Podlaski, F., Filipovic, Z. *et al.* (2004). *In vivo* activation of the p53 pathway by small-molecule antagonists of MDM2. *Science*, **303**, 844–848.
13. Vassilev, L. T. (2004). Small-molecule antagonists of p53–MDM2 binding: research tools and potential therapeutics. *Cell Cycle*, **3**, 419–421.
14. Tovar, C., Rosinski, J., Filipovic, Z., Higgins, B., Kolinsky, K., Hilton, H. *et al.* (2006). Small-molecule MDM2 antagonists reveal aberrant p53 signaling in cancer: implications for therapy. *Proc. Natl. Acad. Sci. USA*, **103**, 1888–1893.
15. Shangary, S., Qin, D., McEachern, D., Liu, M., Miller, R. S., Qiu, S. *et al.* (2008). Temporal activation of p53 by a specific MDM2 inhibitor is selectively toxic to tumors and leads to complete tumor growth inhibition. *Proc. Natl. Acad. Sci. USA*, **105**, 3933–3938.
16. Kubbutat, M. H., Jones, S. N. & Vousden, K. H. (1997). Regulation of p53 stability by Mdm2. *Nature*, **387**, 299–303.
17. Efeyan, A., Ortega-Molina, A., Velasco-Miguel, S., Herranz, D., Vassilev, L. T. & Serrano, M. (2007). Induction of p53-dependent senescence by the MDM2 antagonist nutlin-3a in mouse cells of fibroblast origin. *Cancer Res.* **67**, 7350–7357.
18. Vives, E., Charneau, P., van Rietschoten, J., Rochat, H. & Bahraoui, E. (1994). Effects of the Tat basic domain on human immunodeficiency virus type 1 transactivation, using chemically synthesized Tat protein and Tat peptides. *J. Virol.* **68**, 3343–3353.
19. Vives, E., Brodin, P. & Lebleu, B. (1997). A truncated HIV-1 Tat protein basic domain rapidly translocates through the plasma membrane and accumulates in the cell nucleus. *J. Biol. Chem.* **272**, 16010–16017.
20. Potocky, T. B., Menon, A. K. & Gellman, S. H. (2003). Cytoplasmic and nuclear delivery of a TAT-derived peptide and a beta-peptide after endocytic uptake into HeLa cells. *J. Biol. Chem.* **278**, 50188–50194.
21. Caron, N. J., Quenneville, S. P. & Tremblay, J. P. (2004). Endosome disruption enhances the functional nuclear delivery of Tat-fusion proteins. *Biochem. Biophys. Res. Commun.* **319**, 12–20.

22. Lundberg, M., Wikstrom, S. & Johansson, M. (2003). Cell surface adherence and endocytosis of protein transduction domains. *Mol. Ther.* **8**, 143–150.
23. Shokolenko, I. N., Alexeyev, M. F., LeDoux, S. P. & Wilson, G. L. (2005). TAT-mediated protein transduction and targeted delivery of fusion proteins into mitochondria of breast cancer cells. *DNA Repair (Amst.)*, **4**, 511–518.
24. Del Gaizo, V. & Payne, R. M. (2003). A novel TAT-mitochondrial signal sequence fusion protein is processed, stays in mitochondria, and crosses the placenta. *Mol. Ther.* **7**, 720–730.
25. Matsushita, M., Tomizawa, K., Moriwaki, A., Li, S. T., Terada, H. & Matsui, H. (2001). A high-efficiency protein transduction system demonstrating the role of PKA in long-lasting long-term potentiation. *J. Neurosci.* **21**, 6000–6007.
26. Michl, J., Scharf, B., Schmidt, A., Huynh, C., Hannan, R., von Gizycki, H. *et al.* (2006). PNC-28, a p53-derived peptide that is cytotoxic to cancer cells, blocks pancreatic cancer cell growth *in vivo*. *Int. J. Cancer*, **119**, 1577–1585.
27. Wheeler, Y. Y., Kute, T. E., Willingham, M. C., Chen, S. Y. & Sane, D. C. (2003). Intrabody-based strategies for inhibition of vascular endothelial growth factor receptor-2: effects on apoptosis, cell growth, and angiogenesis. *FASEB J.* **17**, 1733–1735.
28. Williams, B. R. & Zhu, Z. (2006). Intrabody-based approaches to cancer therapy: status and prospects. *Curr. Med. Chem.* **13**, 1473–1480.
29. Imai, S., Mukai, Y., Nagano, K., Shibata, H., Sugita, T., Abe, Y. *et al.* (2006). Quality enhancement of the non-immune phage scFv library to isolate effective antibodies. *Biol. Pharm. Bull.* **29**, 1325–1330.

doi:10.1016/j.jmb.2008.11.053 J. Mol. Biol. (2009) 385, 1221–1229

JMB

Available online at www.sciencedirect.com

ScienceDirect

ELSEVIER

Structure–Function Relationship of Tumor Necrosis Factor (TNF) and Its Receptor Interaction Based on 3D Structural Analysis of a Fully Active TNFR1-Selective TNF Mutant

Yohei Mukai[1,2], Hiroko Shibata[2], Teruya Nakamura[3], Yasuo Yoshioka[2,4], Yasuhiro Abe[2], Tetsuya Nomura[1,2], Madoka Taniai[5], Tsunetaka Ohta[5], Shinji Ikemizu[3], Shinsaku Nakagawa[1], Shin-ichi Tsunoda[2], Haruhiko Kamada[2], Yuriko Yamagata[3] and Yasuo Tsutsumi[1,2]*

[1]*Graduate School of Pharmaceutical Sciences, Osaka University, 1-6 Yamadaoka, Suita, Osaka 565-0871, Japan*

[2]*Laboratory of Pharmaceutical Proteomics, National Institute of Biomedical Innovation, Osaka 567-0085, Japan*

[3]*Graduate School of Pharmaceutical Sciences, Kumamoto University, Kumamoto 862-0973, Japan*

[4]*The Center for Advanced Research and Education in Drug Discovery and Development, Osaka University, 1-6 Yamadaoka, Suita, Osaka 565-0871, Japan*

[5]*Hayashibara Biochemical Laboratories, Inc., 1-2-3 Shimoishii, Okayama 702-8006, Japan*

Received 9 July 2008; received in revised form 21 November 2008; accepted 22 November 2008
Available online 6 December 2008

Edited by I. Wilson

Tumor necrosis factor (TNF) is an important cytokine that suppresses carcinogenesis and excludes infectious pathogens to maintain homeostasis. TNF activates its two receptors [TNF receptor (TNFR) 1 and TNFR2], but the contribution of each receptor to various host defense functions and immunologic surveillance is not yet clear. Here, we used phage display techniques to generate receptor-selective TNF mutants that activate only one TNFR. These TNF mutants will be useful in the functional analysis of TNFR.

Six amino acids in the receptor binding interface (near TNF residues 30, 80, and 140) were randomly mutated by polymerase chain reaction. Two phage libraries comprising over 5 million TNF mutants were constructed. By selecting the mutants without affinity for TNFR1 or TNFR2, we successfully isolated 4 TNFR2-selective candidates and 16 TNFR1-selective candidates, respectively. The TNFR1-selective candidates were highly mutated near residue 30, whereas TNFR2-selective candidates were highly mutated near residue 140, although both had conserved sequences near residues 140 and 30, respectively. This finding suggested that the phage display technique was suitable for identifying important regions for the TNF interaction with TNFR1 and TNFR2. Purified clone R1-6, a TNFR1-selective candidate, remained fully bioactive and had full affinity for TNFR1 without activating TNFR2, indicating the usefulness of the R1-6 TNF mutant in analyzing TNFR1 receptor function.

To further elucidate the receptor selectivity of R1-6, we examined the structure of R1-6 by X-ray crystallography. The results suggested that R31A and R32G mutations strongly influenced electrostatic interaction with TNFR2, and that L29K mutation contributed to the binding of R1-6 to TNFR1. This phage display technique can be used to efficiently construct functional mutants for analysis of the TNF structure–function relationship, which might facilitate *in silico* drug design based on receptor selectivity.

Keywords: TNF; X-ray crystallography; phage display system; TNF mutant; receptor specificity

**Corresponding author.* Department of Toxicology, Graduate School of Pharmaceutical Sciences, Osaka University, 1-6 Yamadaoka, Suita, Osaka 565-0871, Japan. E-mail address: ytsutsumi@phs.osaka-u.ac.jp.

Abbreviations used: TNF, tumor necrosis factor; TNFR, TNF receptor; SPR, surface plasmon resonance; wtTNF, wild-type TNF; PDB, Protein Data Bank.

Introduction

Tumor necrosis factor (TNF) is as an important immunity-modulating cytokine that is required for human body defense against infectious diseases and carcinogenesis.[1] Excess TNF, however, causes various autoimmune diseases, such as rheumatoid arthritis, Crohn's disease, and ulcerative colitis.[2–4] The relationship between TNF and disease deterioration must be unraveled before effective therapies can be developed. Both TNF receptor (TNFR) types TNFR1 and TNFR2, which induce different cell signaling, must be analyzed to better understand the function of TNF. Experiments with TNFR knockout mice have revealed the individual functions of TNFR1 and TNFR2 against viral infection, microbial pathogens, and tumor immunity.[5–8] The lack of one TNFR type, however, can affect the function of the other receptor type and weaken its signaling because the two receptors work together by crosstalk signaling.[9–11] This issue complicates investigations of the individual roles of TNFR1 and TNFR2, and the analysis of TNFR function. Therefore, many researchers have attempted to activate only one receptor using a receptor-selective TNF mutant that does not impair the function of the receptor.

In the past decade, several receptor-selective TNF mutants, which are useful for functional analysis of TNFRs, have been constructed.[12,13] Traditional point mutation methods, however, are labor-intensive because a large number of candidates must be individually assessed; therefore, it has been difficult to successfully isolate the desired mutants.[14–17] In particular, a receptor-selective TNF mutant with full bioactivity was difficult to develop due to the fact that a region on TNF shares a binding affinity for the two different receptors.[18,19] Furthermore, inadequate mutations cause a loss of affinity for both TNFR1 and TNFR2, which has made it difficult to create novel mutants with high selectivity and full bioactivity.[20] Therefore, functional analysis of TNFR using these mutants has not progressed sufficiently.

We previously developed a modified phage display technique that can be used to create desired functional mutant proteins. Using this technique, we have successfully created many mutants with high bioactivity,[21] high *in vivo* stability,[22] and antagonist activity[23] that are suitable for drug development. The advantage of this method is that it allows us to obtain information about specific functions and associated sequences, which is very useful for determining the structure–function relationship of a specific protein. This information will be useful for improving the design of therapeutic mutants.

In the present study, we used the phage display technique to create novel receptor-selective TNF mutants with full bioactivity. Structural information of the mutants was determined by crystallographic analysis, and structural simulation was used to determine a feasible basis for receptor selectivity. These TNF mutants will be useful tools for analyzing TNFR signaling. An understanding of the structure and sequence of these functional mutants, combined with bioinformatics techniques, can potentially lead to the design of a desired functional protein, peptide, or peptide mimic, and thus accelerate the development of novel strategies for analyzing disease-related proteins, such as TNF, and the development of associated therapies.

Results

Library construction and selection of receptor-selective TNF mutants

To create receptor-specific TNF mutants using our phage display system, we prepared two phage libraries, Libraries I and II. Each library contained six amino acids randomized in a receptor binding site suggested by point mutation analysis and X-ray crystallography (Fig. 1).[16,17,24] For construction of the TNF mutant library, a mutant TNF-Lys(−) gene was used as template for polymerase chain reaction (PCR) mutagenesis.[22] Sequence analysis of randomly selected clones indicated that Libraries I and II contained 8.2×10^6 and 5.6×10^6 independent clones, respectively. For selection from the library, several rounds of affinity panning were performed against human TNFR1 or TNFR2 using BIAcore 3000. Potent binders to TNFR1 or TNFR2 were concentrated in the library through this panning procedure. The monoclonal candidates in each library were picked up for enzyme-linked immunosorbent assay (ELISA) screening to confirm their receptor binding specifi-

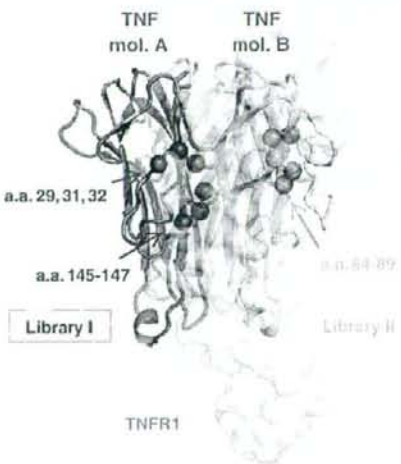

Fig. 1. Positions of randomized residues on the binding interface of the TNF–TNFR1 complex. Mutational residues of Library I (red spheres) and Library II (orange spheres). Green cartoon represents wtTNF. White area represents the surface of the TNFR1 monomer. This binding model structure of the TNF–TNFR1 complex was constructed based on the crystal structure of the LTα–TNFR1 complex (1TNR) and that of wtTNF (1TNF).

Table 1. Substituted residues of TNF mutants from Libraries I and II

			29	31	32	84	85	86	87	88	89	145	146	147
		wtTNF	L	R	R	A	V	S	Y	Q	T	A	E	S
		mutTNF-Lys(−)	—	—	—	—	—	—	—	—	—	—	—	—
TNFR1-selective candidates	Library I (29:32–145:147)	R1-1	I	—	—	—	—	—	—	—	—	—	—	—
		R1-2	Q	—	W	—	—	—	—	—	—	—	—	—
		R1-3	T	G	Y	—	—	—	—	—	—	—	—	—
		R1-4	T	K	Y	—	—	—	—	—	—	—	—	—
		R1-5	T	—	F	—	—	—	—	—	—	—	T	—
		R1-6	K	A	G	—	—	—	—	—	—	—	S	T
	Library II (84:89)	R1-7	—	—	—	S	K	T	—	T	H	—	—	—
		R1-8	—	—	—	S	P	L	—	P	K	—	—	—
		R1-9	—	—	—	S	T	N	—	N	G	—	—	—
		R1-10	—	—	—	T	S	A	—	G	P	—	—	—
		R1-11	—	—	—	T	T	A	—	S	G	—	—	—
		R1-12	—	—	—	T	H	K	—	P	Q	—	—	—
		R1-13	—	—	—	S	K	T	—	S	H	—	—	—
		R1-14	—	—	—	S	S	H	—	R	F	—	—	—
TNFR2-selective candidates	Library I (29:32–145:147)	R2-1	—	—	—	—	—	—	—	—	—	K	D	T
		R2-2	—	—	—	—	—	—	—	—	—	R	T	D
		R2-3	—	—	—	—	—	—	—	—	—	R	E	T
		R2-4	—	—	—	—	—	—	—	—	—	A	D	D
		R2-5	—	—	—	—	—	—	—	—	—	A	N	D

Conserved residues compared with wtTNF are indicated by an em dash (—). Mutated residues in each library are highlighted in gray. Library I included mutated residues 29, 31, 32, and 145–147. Library II contained mutated residues 84–89. R1-1–R1-6 and R1-7–R1-14 were isolated from Libraries I and II, respectively, as TNFR1-selective candidates. TNFR2-selective clones R2-1–R2-5 were isolated from Library I; Library II contained no TNFR2-selective clones.

city. Several clones with TNFR1 or TNFR2 specificity were eventually obtained.

Sequence analysis of receptor-specific TNF mutant candidates

Sequence analysis revealed that we had 14 TNFR1-selective candidates (R1-1–R1-14) and 5 TNFR2-selective candidates (R2-1–R2-5) from Libraries I and II (Table 1). Unfortunately, Library II did not contain any TNFR2-selective mutants. All active TNFR1-selective mutants in Library II retained Tyr87, suggesting that Tyr87 was an essential residue for receptor binding. Analysis of Library I, however, revealed that the mutated and conserved regions of the TNFR1-selective mutants were different from

Table 2. Receptor-selective bioactivities and affinities of TNF mutants

			Relative affinity (% K_d)[a]			Relative bioactivity (% of EC_{50})		
		TNFs	TNFR1	TNFR2	R_1/R_2	HEp2[b]	PC60[c]	R_1/R_2
		wtTNF	100	100	1.0	100	100	1.0
		mutTNF-Lys(−)	108	88	1.2	116	126	0.9
TNFR1-selective candidates	Library I (29:32–145:147)	R1-1	145	121	1.2	492	NT	—
		R1-2	212	32	6.7	436	NT	—
		R1-3	42	18	2.4	343	NT	—
		R1-4	43	3	13.4	447	NT	—
		R1-5	177	2	106.2	582	36	16.2
		R1-6	33	4	8.4	128	<0.07	>1800.0
	Library II (84:89)	R1-7	108	13	8.4	102	NT	—
		R1-8	145	9	16.5	120	173	0.7
		R1-9	175	24	7.4	110	NT	—
		R1-10	149	9	17.0	134	NT	—
		R1-11	219	11	20.4	58	NT	—
		R1-12	51	15	3.5	21	NT	—
		R1-13	51	11	4.6	26	NT	—
		R1-14	46	4	12.0	47	47	1.0
TNFR2-selective candidates	Library I (29:32–145:147)	R2-1	83	112	0.741	12.4	23	0.539
		R2-2	3	143	0.020	0.2	30	0.007
		R2-3	38	225	0.169	2.5	12	0.208
		R2-4	51	572	0.089	6.2	19	0.326
		R2-5	94	324	0.290	13.4	39	0.344

The affinity and bioactivity values are shown as relative values (% wtTNF).

NT, not tested.

[a] Affinity for immobilized TNFR1 and TNFR2 was assessed by SPR using BIAcore 3000.

[b] Human TNFR1-mediated bioactivity was evaluated using a HEp-2 cell cytotoxicity assay. In this assay, HEp-2 cell viability was determined by methylene blue staining. Each value represents the mean±SD.

[c] Human TNFR2-mediated bioactivity was evaluated using PC60-R2 assay. GM-CSF expression by TNFR2-mediated signaling was detected by ELISA. Each value presents the mean±SD.

those of the TNFR2-selective mutants. TNFR1-selective mutants were highly mutated near residue 30 and conserved near residue 140. On the other hand, TNFR2-selective mutants were mutated near residue 140 and conserved near residue 30. This interesting result suggested that the details of the essential binding interface for TNFR1 and TNFR2 differed despite their predicted similar complex forms.[19]

Receptor selectivity and bioactivity of TNF mutants

To investigate the properties of candidate receptor-selective TNF mutants in detail, we prepared recombinant protein using the previously described methods.[21,22] TNF mutants expressed as an inclusion body in *Escherichia coli* were denatured and refolded. Then, active TNF mutants were purified by ion-exchange and gel-filtration chromatography. TNF mutant purity was greater than 90% in sodium dodecyl sulfate–polyacrylamide gel electrophoresis, and all mutants were confirmed to form trimers by gel-filtration analysis (data not shown).

We examined the affinities of these recombinant TNF mutants for TNFR1 and TNFR2 (Table 2). Most of the TNFR1-selective candidates had little affinity for TNFR2 based on surface plasmon resonance (SPR) analysis by BIAcore 3000. In particular, the TNFR1 affinities of R1-2, R1-5, R1-8, R1-9, R1-10, and R1-11 were higher than that of wild-type TNF (wtTNF), despite the loss of their TNFR2 affinities. TNFR1- and TNFR2-mediated bioactivities were assessed by HEp-2 and PC60-hTNFR2 assays, respectively. Interestingly, R1-selective candidates from Library I showed more potent activity via TNFR1 than those from Library II. R1-5 and R1-6 showed superior bioactivity and receptor selectivity. R1-6 was selected as the best overall mutant with greater than 1800-fold selective TNFR1 activity. These mutants were novel because TNFR1-selective mutants with higher bioactivity had not yet been established. Similar studies were performed with the TNFR2-selective candidates. In SPR analysis, these candidates showed higher TNFR2 affinity than wtTNF. Unfortunately, however, none of the TNFR2-selective candidates could sufficiently activate TNFR2 and had less than 40% of the bioactivity of wtTNF.

Next, we performed a competitive binding assay to confirm the details of the TNFR1 selectivity of R1-5 and R1-6—the candidates with the highest selectivity for TNFR1. Competitive affinities were assessed under a certain amount of wtTNF-FLAG, wtTNF fusing FLAG-tag (DYKDDDDK) at C-terminal, as competitor (Fig. 2). Similar to the results of the SPR analysis, R1-5 showed a higher affinity for TNFR1 compared with wild type, and its affinity for TNFR2 was decreased to approximately 10% that for wtTNF, suggesting that R1-5 was a TNFR1-selective mutant. In contrast to the SPR results, however, R1-6 showed a higher competitive affinity for TNFR1, and wtTNF–FLAG binding to TNFR2 was not completely inhibited, even by excess R1-6, which suggested that R1-6

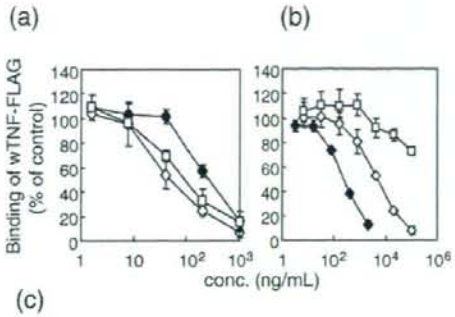

(c)

	TNFR1		TNFR2	
	IC50 (ng/ml)	(%)	IC50 (ngml)	(%)
wtTNF	276.0	100.0	508.1	100.0
R1-5	57.7	478.3	4606.6	11.0
R1-6	105.4	261.9	> 100000.0	< 0.5

Fig. 2. Competitive binding affinities of TNFR1-selective mutants (R1-5 and R1-6). Competitive affinities were assessed under 50 ng/ml FLAG-tagged wtTNF (wtTNF–FLAG) as competitor. Both (a) TNFR1 and (b) TNFR2 were immobilized. Binding of wtTNF–FLAG was inhibited by serially diluted TNF mutants. Final binding of wtTNF–FLAG was assessed by ELISA. Each value represents the mean±SD. (c) IC_{50} values are given as the concentration of the TNF mutant required to inhibit 50% of the maximal binding of wtTNF–FLAG.

lacked binding potency to TNFR2. Because the TNF binding interfaces to the receptors are known to overlap,[19] TNFR1 selectivity caused by a structural change in the R1-6 surface might provide important information for structure-based drug discovery.

X-ray crystallography of TNFR1-selective TNF mutant R1-6

The structural basis of the TNFR1 selectivity of R1-6 was examined by X-ray crystallography. After establishing crystallization conditions, good-quality crystals of R1-6 were obtained (approximately 0.2 mm×0.2 mm×0.3 mm in size). X-ray diffraction data were collected in SPring-8 (a large synchrotron radiation facility in Harima, Japan). Analysis of these data indicated that the space group is *R*3 and that the lattice constants are $a=135.87$ Å, $b=135.87$ Å, and $c=58.02$ Å (Table 3). The R1-6 structure was further refined using the CNS software suite. The results of model validation using the PROCHECK program indicated that there were 86.9% residues in the most favored regions, 13.1% residues in the additionally allowed regions, 0.0% residues in the generously allowed regions, and 0.0% residues in the disallowed regions.

The overall structures of the R1-6 [Protein Data Bank (PDB) code 2ZJC] and wtTNF (PDB code 1TNF) trimers are also similar and superimpose with an rmsd of 1.21 Å for 428 C^{α} atoms (Fig. 3). The structure of

Table 3. Crystallographic parameters and refinement statistics of the R1-6 crystal

Data collection	
Resolution (Å)	50–2.50 (2.59–2.50)
Cell constants (Å)[a]	135.9, 135.9, 58.0
Space group	*R*3
Measured reflections	74,516
Unique reflections	13,445 (1173)
Completeness (%)	99.9 (85.2)
R_{merge} (%)[b]	0.10 (0.53)
$I/\sigma(I)$	28.9 (4.2)
Refinement statistics	
Resolution (Å)	25.67–2.50
Reflections used	12,060
R_{cryst} (%)[c]	20.1
R_{free} (%)[d]	27.2
Completeness (%)	97.1
Atoms	
Protein; water	3338; 59
rmsd from ideality	
Bond lengths (Å); bond angles (°)	0.009; 1.27
Overall *B*-factor (Å^2)	19.7
B-factor rmsd (Å^2)	
Main-chain bonds; side-chain bonds	0.42; 0.77
Main-chain angles; side-chain angles	0.94; 1.48
Ramachandran plot statistics	
Most favored regions (%)	86.9
Additionally allowed regions (%)	13.1
Generously allowed regions (%)	0.0
Disallowed regions (%)	0.0

Values in parentheses are those for the outer shell.

[a] Cell constants are *a*, *b*, and *c*.

[b] $R_{merge} = \sum |I - \langle I \rangle| / \sum \langle I \rangle$, where I is intensity of the observations. R_{merge} in the last shell is high because of the anisotropic mosaicity of the crystal.

[c] $R_{cryst} = \sum ||F_o| - |F_c|| / \sum |F_o|$, where F_o and F_c are the observed and calculated structure factors, respectively.

[d] R_{free} is calculated as for R_{cryst}, but for the test set comprising reflections not used in refinement. The overall *B*-factor was calculated after TLS parameter analysis (TLSANL) using Refmac.

each monomer is similar to each other (rmsd of 0.98–1.12 Å for 140 C^α atoms). Especially, the structures of the β-sheet in each monomer are essentially the same (rmsd of 0.31–0.42 Å for 63 C^α atoms). These features have been found in the wtTNF trimer.[25]

The R1-6 loop structure near mutational residues 31 and 32 is different from that in wtTNF (Fig. 4). This loop structure between monomers is not different (wtTNF: rmsd of 0.61–0.72 Å for 11 C^α atoms; R1-6: rmsd of 0.39–0.91 Å for 11 C^α atoms) (Fig. 4a and b). However, they are clearly different between wtTNF and R1-6 (Fig. 4c). This structural change is thought to be caused by R32G mutation from a sterically bulky arginine residue to a flexible glycine residue. Because this region is close to the TNFR surface, such a structural change in the C^α chain could influence receptor binding. Additional TNF–TNFR docking simulation studies are discussed below.

Discussion

We recently developed the technology to create functional mutant proteins with high bioactivity, high *in vivo* stability, and antagonistic activity.[21–23] Here, we attempted to establish fully bioactive receptor-selective TNF mutants for functional analysis of TNFR1 and TNFR2 using our optimized phage display system. We constructed TNF mutant libraries (Libraries I and II) in which six residues near the receptor binding region were randomized (Fig. 1). From these libraries, we screened for TNFR1- or TNFR2-selective binders, and isolated receptor-selective candidates (Table 1). Despite the successful isolation of TNFR2-selective binders, the TNFR2-selective candidates obtained could not sufficiently activate TNFR2. This result suggested that the production of TNFR2-selective mutants was very rare in our library and that an improved panning method was necessary.

One advantage of our phage-display-based technique is that it can be used to obtain the sequence information of many mutants (Table 1). Tyr87 of TNF was conserved in all mutants obtained from Library II. This residue is highly conserved throughout the TNF superfamily, such as in LTα, LTβ, and LIGHT, and site-directed mutagenesis of the Tyr87 residue of TNF results in a dramatic loss of its biologic activity and its affinities for both TNFR1 and TNFR2.[17] In addition, Tyr87 replacement in antagonistic TNF causes unstable receptor binding and loss of receptor activation in our report.[23] These findings together indicate that Tyr87 is an essential residue for receptor signaling and receptor complex stability.

TNFR1-selective mutants had mutations near residue 30 and conserved residues near residue 140. In contrast, TNFR2-selective mutants had mutations near residue 140 and conserved residues near residue 30. These findings support those of previous point mutation analyses[15–17] and suggest that our phage-

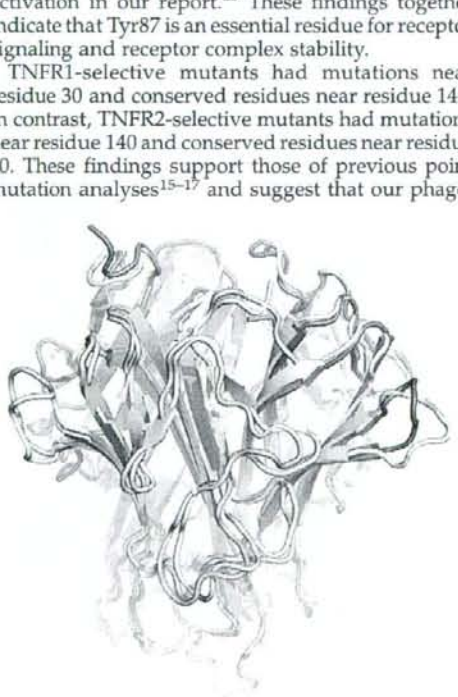

Fig. 3. Overall structure of wtTNF and R1-6. Merge image of previously reported wtTNF structure (green; 1TNF) and refined structure of R1-6 (white; 2ZJC). The flexible loop containing residues 100–110 shown at the bottom of the figure was disordered in the R1-6 structure.

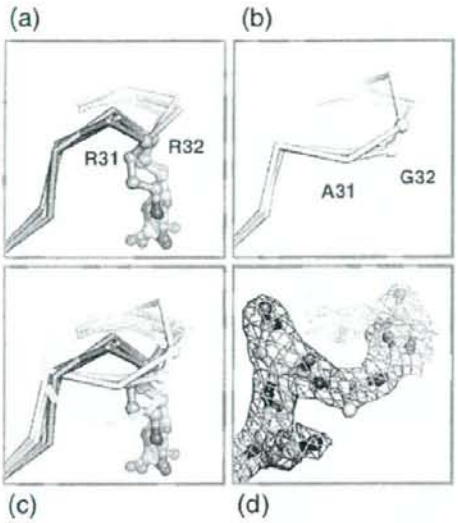

Fig. 4. Structural difference in receptor binding loop between wtTNF and R1-6. Each TNF monomer was superimposed using the CCP4i program. Details of the receptor binding loop, including residues 31 and 32, are shown in these figures. (a) Loops of wtTNF monomers (green); (b) loops of R1-6 monomers (white); (c) merged image of the loops of wtTNF and R1-6; (d) $2F_o-F_c$ map contoured at 1.0σ of R1-6 loop (pink mesh). The different C^α chains are highlighted by the dashed orange circle in (c).

display-based technique can be used to rapidly gather important information about the function–sequence relationships determined by long-term point mutation analysis. In the present study, we successfully isolated mutants that retained TNFR affinity from a huge phage library containing over a million repertoires. Most of the mutants in the library had no TNFR affinity and were therefore discarded through this selection step. This finding may indicate that the mutational residues in these unbound clones diminish TNFR affinity. This method may be useful for examining the function, capability, and sequence–function relationship of unknown cytokines and proteins.

Using these receptor-selective candidates, we expressed recombinant proteins and estimated their bioactivities and affinities for TNFR1 and TNFR2. R1-6, the most highly TNFR1-selective mutant, bound and activated TNFR1 efficiently despite the loss of its affinity for TNFR2. X-ray crystallography of R1-6 revealed that the crystal structure of R1-6 was a trimer (similar to wtTNF), and no other salient differences in the overall structure were observed. Superimposition of wtTNF and R1-6 sequences, however, revealed that the C^α of the receptor binding loop near residue 30 was partially different (Fig. 4). This change might influence the receptor binding mode of R1-6. We further used the superimposition program to perform docking simulations with TNF and TNFR1 based on the crystal structure of the LTα–TNFR1 complex (PDB code 1TNR).[18]

Based on the model wtTNF–TNFR1 complex, Arg31 of TNF would interact electrostatically with Glu56 of TNFR1. The main chain of TNF was too close to His69 of TNFR1, however, potentially causing potential steric hindrance (Fig. 5a). On the other hand, a structural change in the loop in R1-6, however, was thought to solve this problem (Fig. 5b). Arg32 of wtTNF associated with Ser72 of TNFR1 (Fig. 5a). In the R1-6 structure, however, this role of Arg32 was thought to be compensated for by Lys29 (Fig. 5b). This speculation was supported by the crystal structure of the LTα–TNFR1 complex.[18] The position of Lys29 in R1-6 corresponded to that of Arg46 in LTα interacting with Ser72 of TNFR1 by hydrogen bonding. This interesting "compensating role of an amino acid" would be difficult to induce using single point mutation methods, which is another advantage of our modified phage display technique.

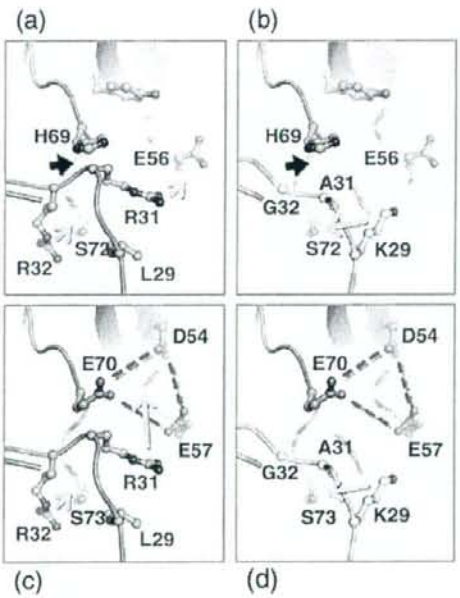

Fig. 5. Model of TNF binding to TNFR1 and TNFR2. Receptor binding interfaces of (a) wtTNF–TNFR1 (green–red); (b) R1-6–TNFR1 (white–red); (c) wtTNF–TNFR2 (green–blue); and (d) R1-6–TNFR2 (white–blue). The TNF–TNFR1 model complex was constructed from 1TNF (wtTNF) and 1TNR (LTα–TNFR1 complex). The predicted TNFR2 structure was constructed by side-chain mutation using the O program. In this simulation, the side chains of each structure were rotated to fit the predicted interaction. Stable structures of these rotamers were constructed using the O program. Steric hindrance might have occurred between His69 of TNFR1 and Arg32 of wtTNF in (a) (black arrowhead). Potential interactions are indicated by orange arrows. A cluster of anionic charged residues (Asp54, Glu57, and Glu70) is highlighted by a broken red line.